

Stochastic Finite Volume Approximation with Clustering in the Parameter Space for Forward Uncertainty Quantification of PDEs with Random Parameters

Zhao Zhang^{a,c,d,*}, Na Ou^{b,*}

^a*Research Centre for Mathematics and Interdisciplinary Sciences, Shandong University, Qingdao, Shandong Province, 266237, China*

^b*School of Mathematics and Statistics, Changsha University of Science and Technology, Changsha, Hunan province, 410114, China*

^c*Frontiers Science Center for Nonlinear Expectations, Minister of Education, Shandong University, Qingdao, Shandong Province, 266237, China*

^d*Suzhou Research Institute of Shandong University, Suzhou, Jiangsu Province, 215123, China*

Abstract

The uncertainty quantification (UQ) for partial differential equations (PDEs) with random parameters is important for science and engineering. Forward UQ quantifies the impact of random parameters on the solution or the quantity-of-interest (QoI). In the current study, we propose a new extension of the stochastic finite volume (SFV) method by clustering samples in the parameter space. Compared to classic SFV based on structured grid in the parameter space, the new scheme based on clustering extends SFV to parameter spaces of higher dimensions. This paper presents the construction of SFV schemes for typical parametric elliptic, parabolic and hyperbolic equations for Darcy flows in porous media, as well as the error analysis, demonstration and validation of the new extension using typical reservoir simulation test cases.

Keywords: uncertainty quantification, stochastic finite volume method, adaptive mesh, clustering, porous media flow

*Corresponding author

Email addresses: zhaozhang@sdu.edu.cn (Zhao Zhang), oyoungla@csust.edu.cn (Na Ou)

1. Introduction

The uncertainty quantification (UQ) of mathematical models approximating physical processes or systems with random parameters is important for accurate and reliable predictions based on the models (Smith, 2013; Oliver et al., 2008). UQ mainly consists of two aspects. The first aspect is forward UQ which concerns the propagation of uncertainty from the random parameters to the outputs of the mathematical model. The other aspect is inverse UQ which concerns the approximation of posterior uncertainty of random parameters given observed data of model outputs.

For forward UQ, the objectives include the computation of the uncertainty of outputs, and the establishment of fast surrogates approximating the physical processes. For inverse UQ, the objective is to compute the reduction of uncertainty in random parameters given observed data. The two aspects of UQ are in fact closely connected through the Bayes' rule, since the likelihood function can be explicitly given or approximated by a surrogate following forward UQ such that the posterior density of random parameters can be conveniently evaluated.

There have been many studies in the area of forward UQ. The stochastic Galerkin method (Lord et al., 2014; Newsum and Powell, 2017) is an intrusive UQ method where the numerical scheme for solving the governing partial differential equations (PDEs) of the physical process need to be modified to a large extent. The resulting linear equation system is very large even for moderate-dimensional problems coupling the physical and parameter spaces spanned by the basis functions. On the other hand, the stochastic collocation method (Xiu, 2010; Yan et al., 2017; Yang et al., 2022) is a non-intrusive UQ method where the forward model can be regarded as a black-box and polynomial chaos expansion is adopted for interpolating the parameter space. Stochastic collocation is more convenient to implement and parallelize compared to stochastic Galerkin. However, both spectral methods rely on smooth polynomials and are hence difficult to approximate discontinuous solutions or those containing sharp interfaces. For this problem, there have been many studies such as the multi-element polynomial chaos, adaptive multiscale finite element, and filtering methods (Maitre et al., 2004; Wan and Karniadakis, 2006; Witteveen and Bijl, 2008; Foo and Karniadakis, 2010; Zhong and Shu, 2022; Vauchel et al., 2023; Xiao et al., 2023). In recent years,

deep learning has been used for surrogate modelling, either data-driven or physics-informed (Zhang, 2022; Zhang et al., 2023). The advantage of deep learning for surrogate modelling is ease-of-implementation and extension to high dimension problems, but the method is not always stable and the optimization of hyperparameters still relies on trials-and-errors in most cases.

The stochastic finite volume (SFV) method proposed firstly in Abgrall (2007) approximate solutions by building grids in the parameter space. SFV only requires little modification of the numerical scheme for the deterministic forward problem, thus is also referred to as a semi-intrusive UQ method (Jin and Pareschi, 2017). The advantage of SFV is that no specific form of the random parameter is required, and discontinuous solutions and those with sharp interfaces can be accurately approximated. However, for even moderate-dimensional random parameters, the computational cost of SFV becomes prohibitively high as the number of grid cells (finite volumes) grows exponentially as the number of dimensions for structured grids in the parameter space (Abgrall et al., 2014; Geraci et al., 2016). Building unstructured grids seem to be a remedy for the problem, but there is yet no algorithms for building unstructured grids in parameter spaces with dimension larger than three.

In the current study, we propose a new SFV scheme based on clustering samples in the parameter space where the clusters can be regarded as unstructured grid cells with implicit boundaries. The conditional expectation in each finite volume is approximated on the samples in the finite volume. The convergence of the new scheme is discussed and validated on test cases of Darcy flows in porous media with random parameters.

The paper is organised as follows. Section 2 presents the development of SFV method. Section 3 presents the new SFV-cluster scheme in the SFV framework by clustering samples in the parameter space. Section 4 presents error analysis. Section 5 shows the test cases. Section 6 is the conclusion remarks.

2. The Stochastic Finite Volume Schemes

2.1. Basic Idea of SFV

Consider a general parametric PDE

$$\mathcal{L}(u, \mathbf{y}) = 0 \text{ ,} \tag{1}$$

where \mathcal{L} is a operator containing initial and boundary conditions, $u = u(\mathbf{x}, t, \mathbf{y})$ is the dependent variable, \mathbf{x} and t are spatial and temporal coordinates, \mathbf{y} is a random parameter that might be dependent on \mathbf{x} and t in some problems. For deterministic PDEs, the idea of finite volume (FV) method is to integrate the governing PDE on each cell in the physical space. For parametric PDEs, the basic idea of SFV is to discretize the parameter space while discretizing the physical space. A set $\{\omega_j\}, j = 1, \dots, N$ is built such that for probability measure P and $\forall i \neq j$, both $P(\omega_i \cap \omega_j) = 0$ and $\Omega = \cup_{j=1}^N \omega_j$ hold. Then, conditional expectations $E(u_h|\omega_j)$ is used to approximate the solution of parametric PDE (Abgrall, 2007), where u_h is the numerical solution in the physical space. The conditional expectation $E(u_h|\omega_j)$ is defined as

$$E(u_h|\omega_j) = \frac{\int_{\omega_j} u_h dP}{\int_{\omega_j} dP} . \quad (2)$$

To compute $E(u_h|\omega_j)$, the governing parametric PDE needs to be integrated on the cells or finite volumes both in the physical and parameter spaces. Jin and Pareschi (2017) presents the derivation of SFV scheme for a basic hyperbolic conservation law. In the current study, we derive the SFV schemes for elliptic, parabolic and hyperbolic PDEs of Darcy flows in porous media.

2.2. SFV scheme for elliptic steady-state single-phase Darcy flow

The governing equation for elliptic steady-state single-phase Darcy flow in porous media is

$$\nabla \left(\frac{K}{\mu} \nabla p \right) = 0 , \quad (3)$$

where $p = p(\mathbf{x}, \mathbf{y})$ is pressure, $K = K(\mathbf{x}, \mathbf{y})$ is permeability assumed to be uncertain and $\mu = \mu(\mathbf{y})$ is dynamic viscosity. Integrating Eq. (3) over the cells (finite volumes) in physical and parameter spaces, dropping the constant μ yields

$$\int_{\omega_j} \int_{\Delta_i} \nabla \left(\frac{K}{\mu} \nabla p \right) \rho(\mathbf{y}) d\mathbf{x} d\mathbf{y} = 0 , \quad (4)$$

where Δ_i and ω_j are the cells in the physical and parameter spaces, respectively. $\rho(\mathbf{y})$ is the probability density function for \mathbf{y} . Adopting finite volume

method on the cell in physical space gives

$$\int_{\omega_j} \sum_c (p_c - p_i) T_{ic} \rho(\mathbf{y}) d\mathbf{y} = 0 \quad (5)$$

where c denotes the neighbouring cells of cell i in the physical space, T_{ic} is the transmissibility between i and c , p_i and p_c are both cell-averaged pressure values. For mass conservation, T_{ic} is evaluated by the harmonic average of T_i and T_c , where $T_i = (KA/\mu d)_i$, A is the face area between i and c , d is the distance from the cell centre of i to the face centre between i and c (Chen et al., 2006). Assuming that pressure is piecewise constant on cells in both physical and parameter spaces, let $p_{i,j}$ denote the pressure value in the i 'th physical and j 'th parameter cell (cell in the parameter space), we have

$$\sum_c (p_{c,j} - p_{i,j}) \int_{\omega_j} T_{ic} \rho(\mathbf{y}) d\mathbf{y} = 0 . \quad (6)$$

A quadrature rule is adopted to approximate the integration of T_{ic} on ω_j as

$$\bar{T}_{ic,j} = \int_{\omega_j} T_{ic} \rho(\mathbf{y}) d\mathbf{y} = \sum_m T_{ic}(\mathbf{y}_m) \rho(\mathbf{y}_m) w_m , \quad (7)$$

where $m = (m_1, \dots, m_q)$ and w_m denote the quadrature nodes and weights in ω_j . Then Eq. (6) can be written as

$$\sum_c (p_{c,j} - p_{i,j}) \bar{T}_{ic,j} = 0 . \quad (8)$$

for each for ω_j and Δ_i . Eq. (8) is coupled for physical cells but decoupled for parameter cells.

2.3. SFV scheme for parabolic transient single-phase Darcy flow

The governing equation for slightly compressible transient single-phase Darcy flow in porous media is

$$\phi c_t \frac{\partial p}{\partial t} = \nabla \cdot \left(\frac{K}{\mu} \nabla p \right) + f , \quad (9)$$

where $c_t = c_t(\mathbf{y})$ is total compressibility, $\phi = \phi(\mathbf{x}, \mathbf{y})$ is porosity, $f = f(\mathbf{x}, \mathbf{y})$ is the source/sink term. Integrating Eq. (9) over cells in space, time and random parameter yields

$$\int_{\omega_j} \int_{t_i} \int_{\Delta_i} \phi c_t \frac{\partial p}{\partial t} \rho(\mathbf{y}) d\mathbf{x} dt d\mathbf{y} = \int_{\omega_j} \int_{t_i} \int_{\Delta_i} (\nabla \cdot (\frac{K}{\mu} \nabla p) + f) \rho(\mathbf{y}) d\mathbf{x} dt d\mathbf{y} , \quad (10)$$

Adopting the finite volume method in the physical space with implicit time integration gives

$$\int_{\omega_j} |\Delta_i| \phi_i c_t \frac{p_i^{n+1} - p_i^n}{\Delta t} \rho(\mathbf{y}) d\mathbf{y} = \int_{\omega_j} \sum_c T_{ic} (p_c^{n+1} - p_i^{n+1}) \rho(\mathbf{y}) d\mathbf{y} + \int_{\omega_j} q_i^{n+1} \rho(\mathbf{y}) d\mathbf{y} , \quad (11)$$

where V_i is the volume of the i 'th grid cell, p_i^n stands for the pressure at the i 'th cell and time step n . $q_i = fV_i$ is the volumetric flow rate that is non-zero at wells and zero elsewhere. Adopting finite volume approximation for p in the parameter space gives

$$|\Delta_i| \frac{p_{i,j}^{n+1} - p_{i,j}^n}{\Delta t} \int_{\omega_j} \phi_i c_t \rho(\mathbf{y}) d\mathbf{y} = \sum_c (p_{c,j}^{n+1} - p_{i,j}^{n+1}) \int_{\omega_j} T_{ic} \rho(\mathbf{y}) d\mathbf{y} + \int_{\omega_j} q_i^{n+1} \rho(\mathbf{y}) d\mathbf{y} . \quad (12)$$

where $p_{i,j}^n$ denotes the pressure value in the i 'th physical and j 'th parameter cell at the n 'th time step. Then quadrature is adopted similarly as in Eq. (7) to calculate mean values $\overline{(\phi_i c_t)_j}$, $\overline{T}_{ic,j}$ and $\overline{q}_{i,j}^{n+1}$ on ω_j to yield the SFV scheme

$$|\Delta_i| \frac{p_{i,j}^{n+1} - p_{i,j}^n}{\Delta t} \overline{(\phi_i c_t)_j} = \sum_c (p_{c,j}^{n+1} - p_{i,j}^{n+1}) \overline{T}_{ic,j} + \overline{q}_{i,j}^{n+1} . \quad (13)$$

2.4. SFV scheme for hyperbolic transient two-phase Darcy flow

The governing equations for slightly compressible transient immiscible two-phase Darcy flow in porous media, neglecting gravity and capillary pressure, are

$$\phi \left[S_\alpha (c_r + c_\alpha) \frac{\partial p}{\partial t} + \frac{\partial S_\alpha}{\partial t} \right] = \nabla \cdot \left(\frac{k_{r\alpha} K}{\mu_\alpha} \nabla p_\alpha \right) + f_\alpha , \quad (14)$$

where α denotes n for non-wetting and w for wetting phase, $S_\alpha = S_\alpha(\mathbf{x}, t, \mathbf{y})$ is phase saturation, $k_{r\alpha} = k_{r\alpha}(S_\alpha)$ is phase relative permeability, $c_r = c_r(\mathbf{y})$ and $c_\alpha = c_\alpha(\mathbf{y})$ are rock and phase compressibility, respectively. Integration over cells in space, time and random parameter yields

$$\int_{\omega_j} \int_{t_i} \int_{\Delta_i} \phi \left[S_\alpha (c_r + c_\alpha) \frac{\partial p}{\partial t} + \frac{\partial S_\alpha}{\partial t} \right] \rho(\mathbf{y}) d\mathbf{x} dt d\mathbf{y} = \int_{\omega_j} \int_{t_i} \int_{\Delta_i} \left[\nabla \left(\frac{k_{r\alpha} K}{\mu_\alpha} \nabla p_\alpha \right) + f_\alpha \right] \rho(\mathbf{y}) d\mathbf{x} dt d\mathbf{y} , \quad (15)$$

Summing up the two equations, we have

$$\int_{\omega_j} \int_{t_i} \int_{\Delta_i} \phi (c_r + S_n c_n + S_w c_w) \frac{\partial p}{\partial t} d\mathbf{x} dt d\mathbf{y} = \int_{\omega_j} \int_{t_i} \int_{\Delta_i} \left[\nabla \left(\left(\frac{k_{rn}}{\mu_n} + \frac{k_{rw}}{\mu_w} \right) K \nabla p \right) + f \right] d\mathbf{x} dt d\mathbf{y} , \quad (16)$$

The finite volume method in the physical space and the implicit-pressure explicit-saturation time integration scheme are adopted. Therefore,

$$\int_{\omega_j} \frac{|\Delta_i| \phi_i c_t}{\Delta t} (p_i^{n+1} - p_i^n) \rho(\mathbf{y}) d\mathbf{y} = \int_{\omega_j} \sum_c \lambda_{ic} T_{ic} (p_c^{n+1} - p_i^{n+1}) \rho(\mathbf{y}) d\mathbf{y} + \int_{\omega_j} q_i^{n+1} \rho(\mathbf{y}) d\mathbf{y} , \quad (17)$$

where $q = f|\Delta_i| = (f_n + f_w)|\Delta_i|$ is the total volumetric flow rate, $\lambda_{ic} = (\lambda_n + \lambda_w)_{ic} = \left(\frac{k_{rn}}{\mu_n} + \frac{k_{rw}}{\mu_w} \right)_{ic}$ is the total mobility evaluated by the first-order upwind scheme. Saturation and flow rates are fixed for computing pressure. Then saturation is updated explicitly as

$$\begin{aligned} \int_{\omega_j} \left[\frac{|\Delta_i| \phi_i S_{w,i}^n c_w}{\Delta t} (p_i^{n+1} - p_i^n) + |\Delta_i| \phi_i \frac{S_{w,i}^{n+1} - S_{w,i}^n}{\Delta t} \right] \rho(\mathbf{y}) d\mathbf{y} = \\ \int_{\omega_j} \sum_c \lambda_{w,ic} T_{ic} (p_c^{n+1} - p_i^{n+1}) \rho(\mathbf{y}) d\mathbf{y} + \int_{\omega_j} q_{w,i}^{n+1} \rho(\mathbf{y}) d\mathbf{y} . \end{aligned} \quad (18)$$

Assuming pressure and saturation are piecewise constant on cells in both physical and parameter spaces, letting $S_{w,i,j}^n$ denote the saturation of the wetting phase in the i 'th physical and j 'th parameter cell at the n 'th time step, and adopting quadrature similarly as Eq. (7) to compute mean values $\overline{\phi_{i,j}}$, $\overline{(\phi_i c_t)_j}$, $\overline{(\phi_i c_w)_j}$, $\overline{(\lambda_{w,ic} T_{ic})_j}$, $\overline{q_{i,j}^{n+1}}$ and $\overline{q_{w,i,j}^{n+1}}$ on ω_j to yield the SFV scheme

$$\frac{|\Delta_i| \overline{(\phi_i c_t)_j}}{\Delta t} (p_{i,j}^{n+1} - p_{i,j}^n) = \sum_c \overline{(\lambda_{w,ic} T_{ic})_j} (p_{c,j}^{n+1} - p_{i,j}^{n+1}) + \overline{q_{i,j}^{n+1}} , \quad (19)$$

$$\frac{|\Delta_i|(\overline{\phi_i c_w})_j S_{w,i,j}^n}{\Delta t} (p_{i,j}^{n+1} - p_{i,j}^n) + |\Delta_i| \bar{\phi}_{i,j} \frac{S_{w,i,j}^{n+1} - S_{w,i,j}^n}{\Delta t} = \sum_c \overline{(\lambda_{w,ic} T_{ic})_j} (p_{c,j}^{n+1} - p_{i,j}^{n+1}) + \bar{q}_{w,i,j}^{n+1}. \quad (20)$$

3. A New SFV-Cluster Scheme

In this section, we develop a new SFV-cluster scheme in the SFV framework by clustering samples in the parameter space. The SFV method is based on the discretisation of physical and parameter spaces. The existing schemes of SFV employ structured meshes in the parameter space, while the adaptivity approach allows anisotropic mesh resolution. As a consequence of structured mesh generation, the number of grid cells, as well as the computational cost of SFV, grows exponentially as the number of dimensions in the parameter space. This restricts SFV to UQ problems of low dimensions. An obvious remedy for this problem is to build unstructured mesh in the parameter space. However, there is no algorithm yet for generating unstructured mesh in high or even moderate-dimensional spaces.

An important observation of SFV is that the cells (finite volumes) in the parameter space are decoupled, indicating that there is no flux across the boundary faces between them. The quadrature rule is based on the nodes (samples) in the parameter space, and what matters is which samples belong to each cell. Therefore, we can approximate the parameter space by an array of samples, and then cluster the samples into different clusters/groups. Each cluster is regarded as a cell with implicit boundary in the parameter space. This allows us to generate unstructured mesh with implicit boundaries for SFV in spaces with dimension larger than 3 conveniently. Suppose a number of N samples are generated by the Monte Carlo method, and cell (group) ω_j contains m samples, then we have $\rho(\mathbf{y}_m) = 1/N$ and $|\omega_j| = m/N$. Further, let $w_m = 1$ for simplicity, Eq. (7) becomes

$$\bar{T}_{ic,j} = \frac{1}{N} \sum_{\mathbf{y}_m \in \omega_j} T_{ic}(\mathbf{y}_m). \quad (21)$$

which is used to estimate the integration of $T_{ic,j}$ on cell ω_j in the parameter space.

4. Error analysis

Assume $p = p(x, t; y)$ is the exact solution to the PDE and p_{ik}^n is its approximation at a fixed time moment $t = t^n$ resulting from SFVM. We denote it as $p_h = \{p_{ik}^n\}$. Let the mean and variance of the exact solution at the point (x_i, t_n) be

$$\begin{aligned}\mathbb{E}[p](x_i, t^n) &= \int_{\Omega} p(x_i, t^n; y) \rho(y) dy, \\ \mathbb{V}[p](x_i, t^n) &= \mathbb{E}[p^2(x_i, t^n)] - (\mathbb{E}[p](x_i, t^n))^2,\end{aligned}$$

respectively. Denote

$$\begin{aligned}\mathbb{E}[p_h]_i^n &= \int_{\Omega} \sum_k^{N_y} p_{ik}^n \rho(y) dy, \\ \mathbb{V}[p_h]_i^n &= \mathbb{E}[p_h^2]_i^n - (\mathbb{E}[p_h]_i^n)^2,\end{aligned}$$

the corresponding SFVM-Cluster approximation is computed as follows:

$$\begin{aligned}E_h[p_h]_i^n &= \sum_{k=1}^{N_y} p_{ik}^n \tilde{\alpha}_k, \\ V_h[p_h]_i^n &= E_h[p_h^2]_i^n - (E_h[p_h]_i^n)^2,\end{aligned}$$

where $\tilde{\alpha}_k$ is the numerical approximation of α_k and

$$\begin{aligned}\alpha_k &= \int_{\omega_k} \rho(y) dy, \\ \tilde{\alpha}_k &= \frac{1}{N} \sum_{n=1}^N \mathbb{K}(y_n \in \omega_k),\end{aligned}$$

according to the Monte Carlo approximation, the error between $\tilde{\alpha}_k$ and α_k is

$$|\alpha_k - \tilde{\alpha}_k| \lesssim O\left(\frac{\sigma_k}{\sqrt{N}}\right),$$

where σ_k is the standard variance of the random variable $\mathbb{K}(y \in \omega_k)$. We use the moment estimator to estimate the value of σ_k , denote the random variable $Z = \mathbb{K}(y \in \omega_k)$, then the zero-order moment estimate is

$$\bar{z} = \frac{m_k}{N},$$

where m_k is the number of points belonging to the k -th cluster. We can then have the second-order moment estimate

$$\begin{aligned} s_k^2 &= \frac{1}{N-1} \sum_{i=1}^N (z_i - \bar{z})^2 \\ &= \frac{1}{N-1} \left(\sum_{i=1}^{m_k} \left(1 - \frac{m_k}{N}\right)^2 + \sum_{i=1}^{N-m_k} \left(0 - \frac{m_k}{N}\right)^2 \right) \\ &= \frac{(N-m_k)m_k}{N(N-1)}, \end{aligned}$$

which is an unbiased estimate of σ_k^2 . When $m_k < N/2$, the less points contained in the k -th cluster, the smaller the estimated σ_k is.

Let p_h^y be the numerical solution which is exact in x variable and discretized in y and by p_h^{xy} the numerical discretized in both variables. Assume that

$$\begin{aligned} \|p_h^y - p_h^{xy}\|_{L^1(D)} &\leq C_1 \Delta x^q, \quad \forall y \in \Omega, \\ \|p - p_h^y\|_{L^1(\Omega)} &\leq C_2 \Delta y^r, \quad \forall x \in D, \end{aligned}$$

where Δx is the mesh size in the physical domain, Δy can be viewed as the largest radius of the clusters, which is used to measure the 'discretization' error in the parameter space. Then the following estimates are established:

Theorem 4.1. *The error of the expectation and variance are*

$$\begin{aligned} \|\mathbb{E}[p] - E_h[p_h^{xy}]\|_{L^1(D)} &\leq C_1 \Delta x^q + C \Delta y^r + C_3 \frac{\sigma}{\sqrt{N}}, \\ \|\mathbb{V}[p] - V_h[p_h]\|_{L^1(D)} &\leq C'_1 \Delta x^q + C' \Delta y^r + C'_3 \frac{\sigma}{\sqrt{N}}. \end{aligned}$$

Proof.

$$\begin{aligned} \|\mathbb{E}[p] - E_h[p_h^{xy}]\|_{L^1(D)} &= \|\mathbb{E}[p] - \mathbb{E}[p_h^y] + \mathbb{E}[p_h^y] - \mathbb{E}[p_h^{xy}] + \mathbb{E}[p_h^{xy}] - E_h[p_h^{xy}]\|_{L^1(D)} \\ &\leq \|\mathbb{E}[p] - \mathbb{E}[p_h^y]\|_{L^1(D)} + \|\mathbb{E}[p_h^y] - \mathbb{E}[p_h^{xy}]\|_{L^1(D)} \\ &\quad + \|\mathbb{E}[p_h^{xy}] - E_h[p_h^{xy}]\|_{L^1(D)}, \end{aligned}$$

for the first integral, we have

$$\begin{aligned} \|\mathbb{E}[p] - \mathbb{E}[p_h^y]\|_{L^1(D)} &= \int_D \left| \int_{\Omega} (p - p_h^y) \rho(y) dy \right| dx \leq \int_D \sup_{\Omega} \rho(y) \int_{\Omega} |p - p_h^y| dy dx \\ &= \sup_{\Omega} \rho(y) \int_D \|p - p_h^y\|_{L^1(\Omega)} dx \leq \sup_{\Omega} \rho(y) |D| C_2 \Delta y^r \leq C \Delta y^r, \end{aligned}$$

where $|D|$ is the area of the physical domain. Similarly, for the second integral, we have

$$\begin{aligned}
\|\mathbb{E}[p_h^y] - \mathbb{E}[p_h^{xy}]\|_{L^1(D)} &= \int_D \left| \int_{\Omega} (p_h^y - p_h^{xy}) \rho(y) dy \right| dx \\
&= \int_{\Omega} \left[\int_D |p_h^y - p_h^{xy}| dx \right] \rho(y) dy \\
&= \int_{\Omega} \|p_h^y - p_h^{xy}\|_{L^1(D)} \rho(y) dy \\
&\leq C_1 \Delta x^q \int_{\Omega} \rho(y) dy \leq C_1 \Delta x^q
\end{aligned}$$

the third term can be estimated as

$$\begin{aligned}
|\mathbb{E}[p_h]_i^n - E_h[p_h]_i^n| &= \left| \sum_k p_{ik}^n (\alpha_k - \tilde{\alpha}_k) \right| \\
&\lesssim \frac{\sigma}{\sqrt{N}} \sum_k |p_{ik}^n|,
\end{aligned}$$

then

$$\|\mathbb{E}[p_h^{xy}] - E_h[p_h^{xy}]\|_{L^1(D)} \lesssim \frac{\sigma}{\sqrt{N}} \|p_h^{xy}\|_{L^1(D \times \Omega)},$$

hence

$$\|\mathbb{E}[p] - E_h[p_h^{xy}]\|_{L^1(D)} \leq C_1 \Delta x^q + C \Delta y^r + C_3 \frac{\sigma}{\sqrt{N}}.$$

For the variance,

$$\begin{aligned}
\|\mathbb{V}[p] - V_h[p_h^{xy}]\|_{L^1(D)} &\leq \left\| \mathbb{E}[p^2] - E_h[(p_h^{xy})^2] \right\|_{L^1(D)} + \left\| (\mathbb{E}[p])^2 - (E_h[p_h^{xy}])^2 \right\|_{L^1(D)} \\
&\leq \left\| \mathbb{E}[p^2] - \mathbb{E}[(p_h^{xy})^2] \right\|_{L^1(D)} + \left\| \mathbb{E}[(p_h^{xy})^2] - E_h[(p_h^{xy})^2] \right\|_{L^1(D)} \\
&\quad + \left\| (\mathbb{E}[p])^2 - (E_h[p_h^{xy}])^2 \right\|_{L^1(D)}
\end{aligned}$$

the first term can be estimated by

$$\begin{aligned}
\left\| \mathbb{E} [p^2] - \mathbb{E} [(p_h^{xy})^2] \right\|_{L^1(D)} &= \int_D \left| \int_{\Omega} [p^2 - (p_h^{xy})^2] \rho(y) dy \right| dx \leq \int_D \int_{\Omega} |p^2 - (p_h^{xy})^2| \rho(y) dy dx \\
&= \int_D \int_{\Omega} |p - p_h^{xy}| |p + p_h^{xy}| \rho(y) dy dx \leq C \int_D \int_{\Omega} |p - p_h^{xy}| \rho(y) dy dx \\
&\leq C \int_D \int_{\Omega} |p - p_h^y| \rho(y) dy dx + C \int_D \int_{\Omega} |p_h^y - p_h^{xy}| \rho(y) dy dx \\
&\leq C \sup_{\Omega} \rho(y) \int_D dx \int_{\Omega} |p - p_h^y| dy + C \int_{\Omega} \rho(y) dy \int_D |p_h^y - p_h^{xy}| dx \\
&= C \sup_{\Omega} \rho(y) \int_D \|p - p_h^y\|_{L^1(\Omega)} dx + C \int_{\Omega} \|p_h^y - p_h^{xy}\|_{L^1(D)} \rho(y) dy \\
&\leq C \sup_{\Omega} \rho(y) |D| C_2 \Delta y^r + C C_1 \Delta x^q,
\end{aligned}$$

for the second integral, we have

$$\begin{aligned}
|\mathbb{E} [(p_h^{xy})^2]_i^n - E_h [(p_h^{xy})^2]_i^n| &= \left| \int_{\Omega} \sum_k (p_{ik}^n)^2 \rho(y) dy - \sum_k (p_{ik}^n)^2 \tilde{\alpha}_k \right| \\
&\leq \sum_k (p_{ik}^n)^2 \left| \left(\int_{\omega_k} \rho(y) dy - \tilde{\alpha}_k \right) \right| \\
&\lesssim \frac{\sigma}{\sqrt{N}} \sum_k (p_{ik}^n)^2
\end{aligned}$$

hence

$$\left\| \mathbb{E} [(p_h^{xy})^2] - E_h [(p_h^{xy})^2] \right\|_{L^1(D)} \lesssim \|(p_h^{xy})^2\|_{L^1(D \times \Omega)} \frac{\sigma}{\sqrt{N}} \leq C \frac{\sigma}{\sqrt{N}}.$$

For the third integral, we get

$$\begin{aligned}
\left\| (\mathbb{E}[p])^2 - (E_h[p_h^{xy}])^2 \right\|_{L^1(D)} &= \int_D \left| (\mathbb{E}[p])^2 - (E_h[p_h^{xy}])^2 \right| dx \\
&= \int_D |\mathbb{E}[p] - E_h[p_h^{xy}]| |\mathbb{E}[p] + E_h[p_h^{xy}]| dx, \\
&\leq C \|\mathbb{E}[p] - E_h[p_h^{xy}]\|_{L^1(D)},
\end{aligned}$$

finally,

$$\|\mathbb{V}[p] - V_h[p_h^{xy}]\|_{L^1(D)} \leq C'_1 \Delta x^q + C' \Delta y^r + C'_3 \frac{\sigma}{\sqrt{N}}.$$

□

The proofs are analogous to the ones in (Jin and Pareschi, 2017), more details can be found there. From Theorem 4.1, we know that

$$\|\mathbb{E}[p] - E_h[p_h^{xy}]\|_{L^1(D)} \leq C_1 \Delta x^q + C \Delta y^r + C_3 \frac{\sigma}{\sqrt{N}}. \quad (22)$$

We also know that

$$\sigma^2 \approx s_k^2 = \frac{(N - m_k)m_k}{N(N - 1)}$$

Therefore, assuming $m_k = N/N_y$ where N_y is the number of clusters in the parameter space, we have approximately

$$\sigma < \sqrt{\frac{N}{N - 1}} \frac{1}{\sqrt{N_y}} \quad (23)$$

Assuming that $\Delta y^r = V/N_y$, from Eq. (22), we have

$$\|\mathbb{E}[p] - E_h[p_h^{xy}]\|_{L^1(D)} \leq C_1 \Delta x^q + C_2 \frac{1}{N_y} + C_3 \frac{1}{\sqrt{(N - 1)N_y}} \quad (24)$$

Therefore, for a fixed N , the error of expectation is $\mathcal{O}(1/N_y)$, if the samples are distributed in the parameter space evenly and the clustering algorithm can partition the samples in the parameter space equally well. The error of the variance of SFV can be analyzed similarly.

5. Test Cases

5.1. Single-Phase Steady-State Darcy Flow with 2D Random Parameter

In this test case, we consider the UQ of single-phase steady-state Darcy flow governed by Eq. (3) with random permeability using an idealized model. The physical domain is 200×200 discretized by a 20×20 Cartesian grid. The viscosity μ is set to be unity, while the random permeability is assumed to be 2D that each half of the domain has a homogeneous isotropic but random permeability given by

$$k(x, y) \sim \begin{cases} T(\mu, \sigma, a, b), & x < 100 \\ U(c, d), & x \geq 100 \end{cases} \quad (25)$$

where $T(\mu, \sigma, a, b)$ is truncated normal distribution with mean $\mu = 15$, standard deviation $\sigma = 3$ bounded by $a = 10$ and $b = 20$, $U(c, d)$ is uniform distribution in interval $[c, d]$ with distribution uncertainty such that $[c, d] = [1, 11]$

or [21, 31] with 50% possibility each. Therefore, the parameter space is discontinuous. For simulation, Dirichlet boundary condition $p = 0$ and $p = 1$ are at two corners of the physical domain. Figs. 1a and 1b visualizes one realisation of the random permeability field and the corresponding steady-state pressure field.

The aim is to estimate the mean and variance of the pressure of the 20'th cell located at the bottom-right corner in the domain, which is regarded as the QoI. The straightforward option is the Monte Carlo (MC) method. Given N realisations of the random permeability field, the forward simulation is conducted for each realisation to generate N pressure field, then the mean and variance of p^{20} are computed as

$$\bar{p}^{20} = \frac{1}{N} \sum_{i=1}^N p_i^{20} \quad (26)$$

$$var(p^{20}) = \frac{1}{N-1} \sum_{i=1}^N (p_i^{20} - \bar{p}^{20})^2 \quad (27)$$

The drawback of MC is that a large number of forward simulation runs are needed. In SFV, a number of $N_c < N$ cells are built in the parameter space by clustering samples, then the mean and variance of p^{20} are computed as

$$\bar{p}^{20} = \frac{1}{N_c} \sum_{i=1}^{N_c} p_i^{20} W_i \quad (28)$$

$$var(p^{20}) = \frac{1}{N_c} \sum_{i=1}^{N_c} (p_i^{20} - \bar{p}^{20})^2 W_i \quad (29)$$

where the weight W_i is equal to the probability mass on the i 'th cell computed as

$$W_i = \frac{m}{N} \quad (30)$$

assuming that the i 'th cell contains m samples.

In the current study, a total of 20000 samples are drawn to represent the sample space. Both MC and SFV are conducted to approximate the mean and standard deviation of the QoI which is p^{20} . In theory, the convergence rate of MC and SFV are $\mathcal{O}(1/\sqrt{N})$ and $\mathcal{O}(1/N_y)$, respectively (Jin and Pareschi, 2017). As we tested, the convergence rate of SFV is much faster than MC considering the mean value of averaged pressure of all cells

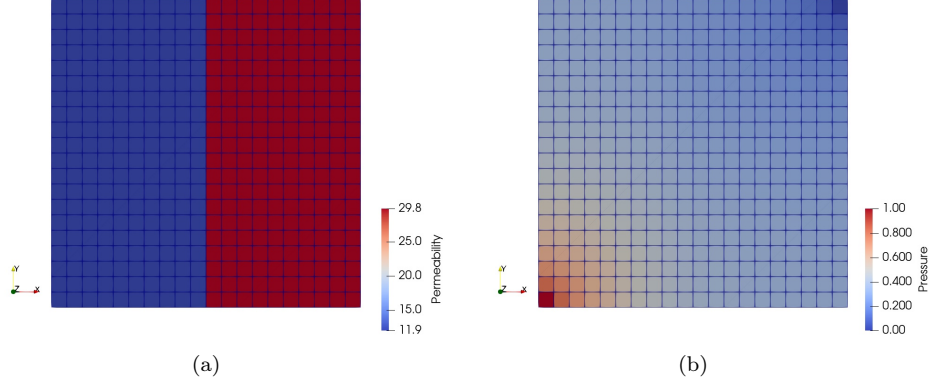


Figure 1: A realisation of the random permeability field for the single-phase steady-state Darcy flow example (a) and the corresponding steady-state pressure field (b).

and the associated standard deviation. The results are compared in Figs. 2 and 3, where for SFV an isotropic Cartesian grid is built in the 2D parameter space with increasing resolution. The convergence of SFV using Cartesian grid or samples clusters as cells in the parameter space is compared in Fig. 4 showing that the SFV scheme using samples' clusters has a slightly higher convergence rate since the clusters are more focused on the areas of higher probability density, compared to Cartesian grid of homogeneous resolution.

5.2. Single-Phase Transient Darcy Flow with 10D Random Parameter

In this test case, we consider the UQ of single-phase transient Darcy flow governed by Eq. (9) with random permeability field. All other parameters are constant scalars summarised in Table 1. A more practical example is considered such that the parameters and variables are with units. The physical domain for the petroleum reservoir is $200 \text{ m} \times 200 \text{ m}$ discretized by a 20×20 Cartesian grid. Initially, all physical cells are at pressure $P_{init} = 30 \text{ MPa}$. Then, the well at a corner starts to produce oil at constant bottom-hole pressure. The process is simulated by the finite volume method in MC or by SFV for 120 time steps with $dt = 10^5$ seconds. The Peaceman's well model is adopted to connect the well-block pressure p^t , the bottom-hole pressure bhp and volumetric flow rate q^t at the time step t for the cell containing the producing well by

$$q^t = PI \cdot (p^t - bhp) . \quad (31)$$

where PI stands for production index.

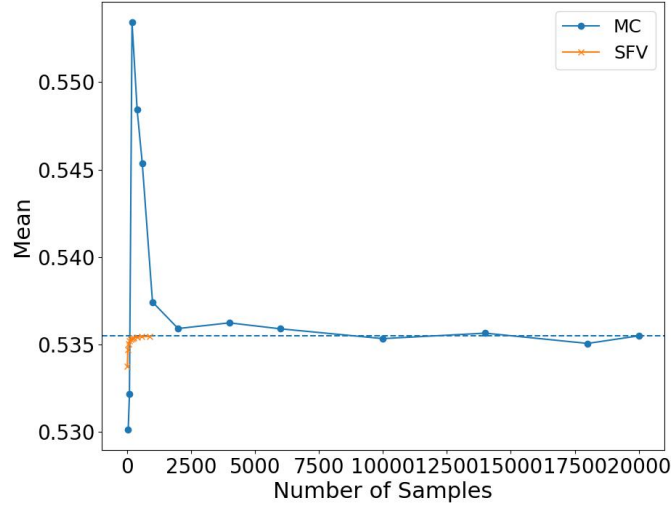


Figure 2: Mean value for p^{20} computed by MC over realisations and by SFV over cells in the parameter space in the steady-state test case. An isotropic Cartesian grid is built in the 2D parameter space for SFV.

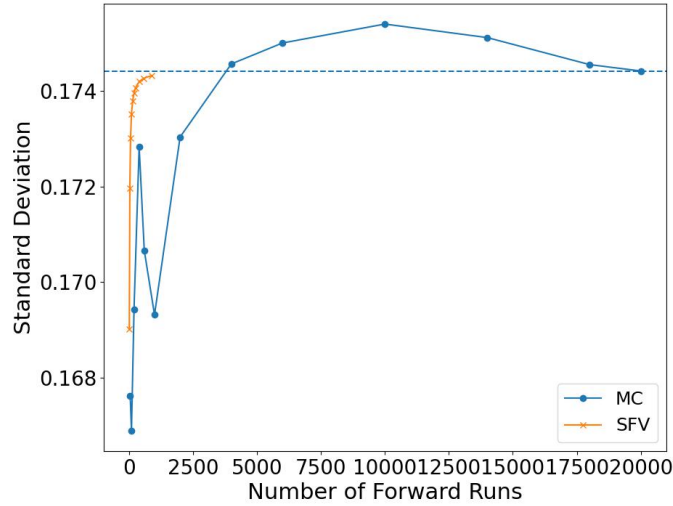


Figure 3: Standard deviation for p^{20} computed by MC over realisations and by SFV over cells in the parameter space in the steady-state test case.

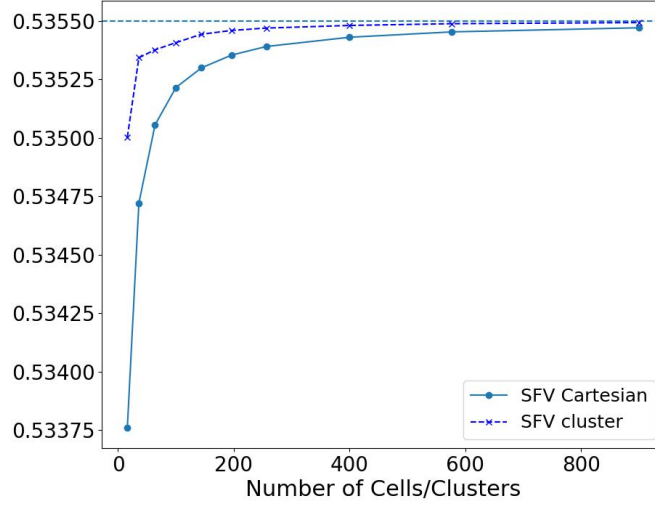


Figure 4: Comparison between the convergence of mean p^{20} for SFV schemes using Cartesian or sample clusters in the parameter space.

Parameter	Value
Porosity	10%
Total Compressibility	$5 \times 10^{-8} \text{ Pa}^{-1}$
Dynamic Viscosity	0.002 Pa*s
Production index	
Bottom-hole pressure	20 MPa

Table 1: A summary of physical parameters.

The physical domain consists of 10 channels, each having a homogeneous but uncertain permeability value. Therefore, the random permeability vector is of dimension 10. The permeability of each dimension follows a uniform distribution with uncertainty. For the i 'th channel, the distribution is $U(i + 1, 5(i + 1))$ mD with 50% possibility, and $U(10(i + 1), 15(i + 1))$ mD with 50% possibility.

For MC, a total of 20000 realisations are generated for the random permeability field which are simulated to estimate the mean and standard deviation of accumulated oil production equal to the total volume of oil produced over the simulation period. One realisation of the permeability field and the corresponding pressure field at end of simulation are shown in Fig. 5. For SFV, the cells/clusters in the parameter space are built by clustering the MC samples using Kmeans algorithm. The simulated flow rates over time for MC realisations and SFV clusters are presented in Fig. 6. It is obvious in Fig. 7 and 8 that the convergence rate of SFV is much faster than MC in terms of mean and standard deviation for the accumulated oil production.

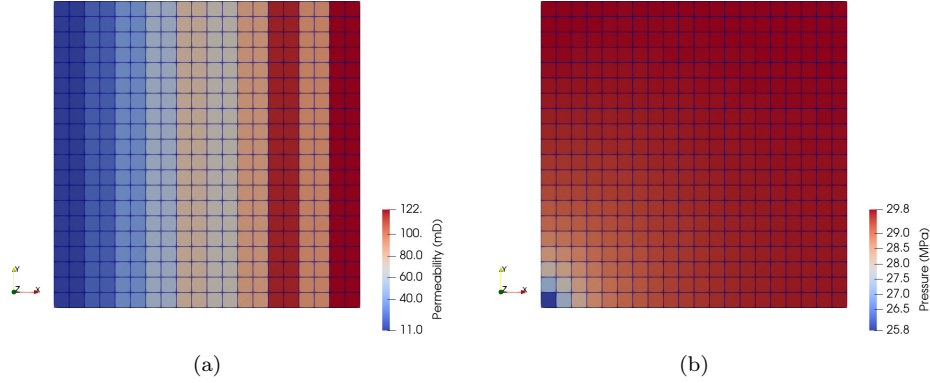


Figure 5: A realisation of the random permeability field for the single-phase transient Darcy flow test case (a) and the corresponding pressure field at end of simulation (b).

5.3. Two-Phase Transient Darcy Flow with 10D Random Parameter

In this test case, we consider the UQ of two-phase transient incompressible Darcy flow governed by Eq. (14) with random permeability field. Similarly as the last example, the physical domain is composed of 10 channels with random permeability. All other physical parameters are constant scalars summarised in Table 2. The permeability of each dimension follows a uniform

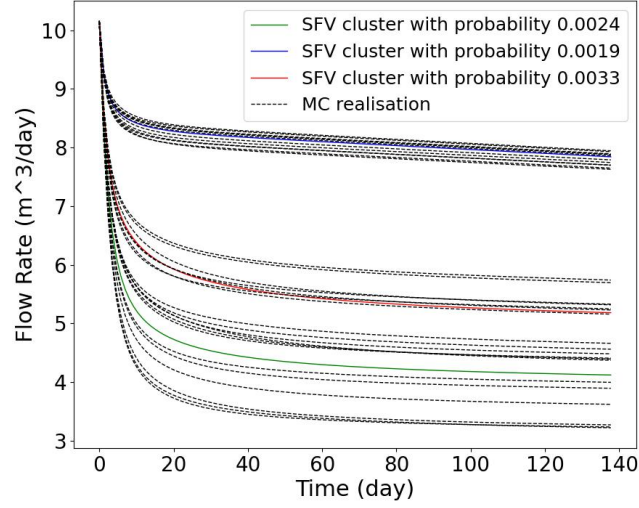


Figure 6: The flow rates over time of some MC realisations and SFV clusters for the single-phase transient Dary flow test case.

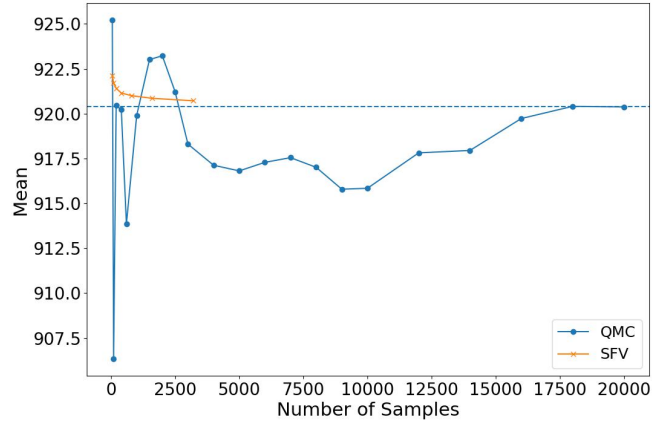


Figure 7: Mean value for the accumulated oil production computed by MC over realisations and by SFV over cells/clusters in the parameter space. The cells/clusters are built by Kmeans over MC samples.

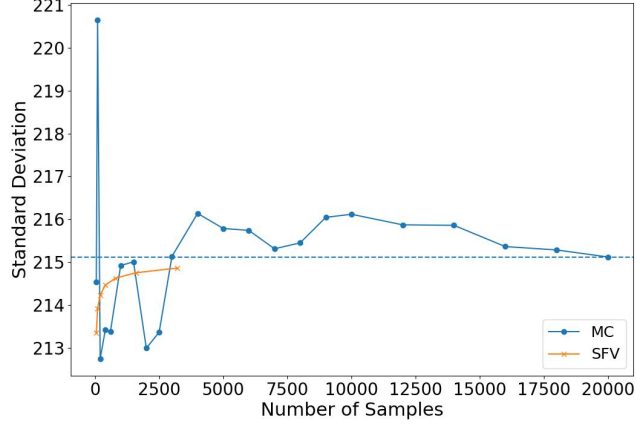


Figure 8: Standard deviation for the accumulated oil production computed by MC over realisations and by SFV over cells/clusters in the parameter space. The cells/clusters are built by Kmeans over MC samples.

distribution with uncertainty. For the i 'th channel, the distribution is $U(i + 1, 2(i + 1))$ mD with 50% possibility, and $U(3(i + 1), 6(i + 1))$ mD with 50% possibility.

The size and grid for the physical domain is the same as the last example. Dirichlet boundary conditions of 30 and 26 MPa are set at two corners (top-right and bottom-left) of the domain. The reservoir is initially at irreducible water saturation, and is swept by water from the top-right corner of higher Dirichlet boundary condition. Fig. 9 visualises one realisation of the random permeability field and the corresponding water saturation field at end of simulation. For simulation, there are 1500 time steps with $dt = 80$ hours.

The QoI for UQ is the mean and standard deviation for the swept volume by injected water. The swept volume is computed as $\sum_{i=1}^N (S_{w,i} - S_{iw}) * V_i$ where $S_{w,i}$ is the water saturation of the i 'th cell in the physical grid, S_{iw} is the irreducible water saturation and V_i is the volume of the i 'th cell. For MC, 10000 realisations are used to estimate the mean and standard deviation for the swept volume. For SFV, clusters are built on 32000 realisations to serve as cells in the parameter space. For small number of forward simulation runs as shown in Figs. 10 and 11, the convergence of SFV is more steady and the UQ results of SFV are more reliable.

Parameter	Value
Porosity	20%
Water Dynamic Viscosity	0.001 Pa*s
Oil Dynamic Viscosity	0.0018 Pa*s
Irriducible Water Saturation	0.2

Table 2: A summary of physical parameters for the two-phase transient Darcy flow example.

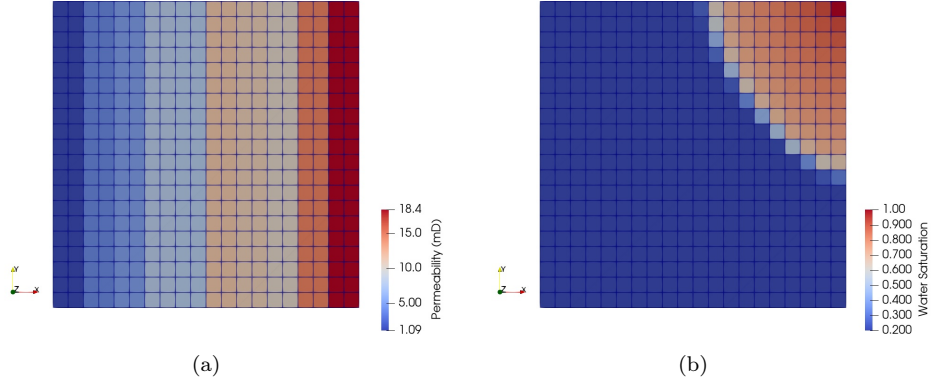


Figure 9: A realisation of the random permeability field for the two-phase transient Darcy flow test case (a) and the corresponding water saturation field at end of simulation (b).

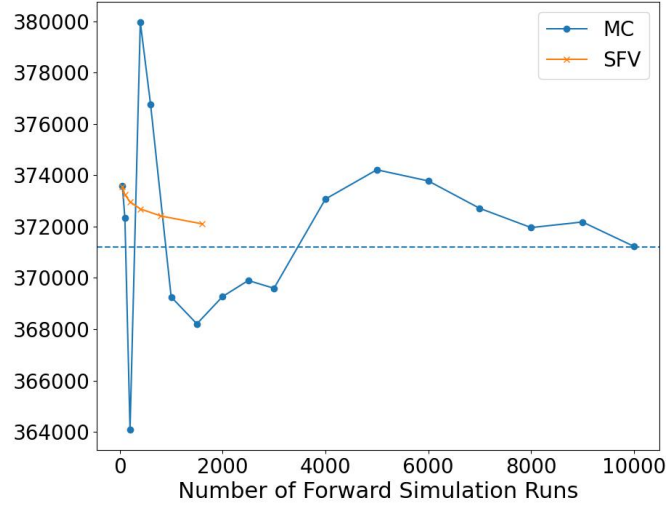


Figure 10: Mean value for the swept volume computed by MC over realisations and by SFV over cells/clusters in the parameter space. The cells/clusters are built by Kmeans over MC samples.

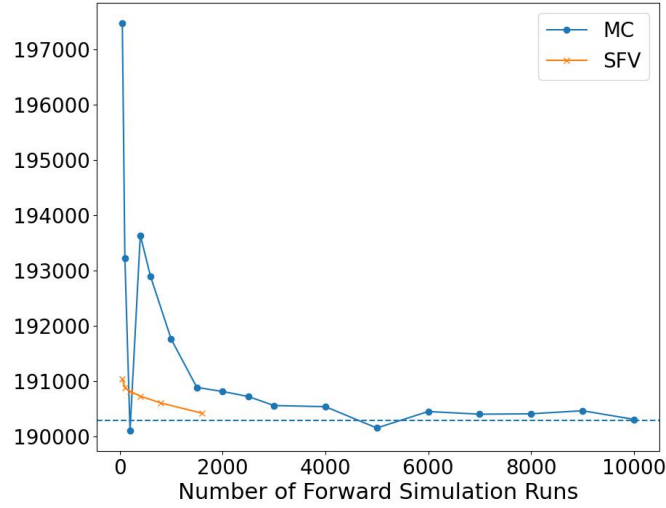


Figure 11: Standard deviation for the swept volume computed by MC over realisations and by SFV over cells/clusters in the parameter space. The cells/clusters are built by Kmeans over MC samples.

6. Conclusions

In the current study, we propose a new SFV-cluster scheme in the SFV framework by clustering samples in the parameter space. Since there is no flux between cells in the parameter space assuming first-order SFV, the cells are decoupled entirely. Therefore, we can build unstructured mesh with implicit boundaries in the parameter space by clustering MC samples where the clusters are treated as cells. Assisted by the new SFV-cluster scheme, we only need to conduct forward simulation on the clusters, thus reducing the number of simulation runs for estimating the mean and variance. Error analysis for the new scheme has been presented, and the new scheme has been validated on elliptic, parabolic and hyperbolic PDEs with random parameters. The new SFV scheme can be used on MC samples to evaluate the mean and variance efficiently, especially when the number of forward simulations is limited. For extension to parameter spaces of higher dimensions, linear or nonlinear manifold learning could be used for dimension reduction such that clustering can be conducted accurately.

Acknowledgements

The research is supported by the Natural Science Foundation of Shandong Province (No. ZR2021QE105, No. ZR2024MA057), the Natural Science Foundation of Jiangsu Province (No. BK20220272), Qingdao Science and Technology Bureau (23-1-2-qljh-3-gx) and the Future Plan for Young Scholars of Shandong University. Na Ou acknowledges the support of Chinese NSF 11901060, Hunan Provincial Natural Science Foundation of China 2021JJ40557.

References

- Abgrall, R., 2007. A simple, flexible and generic deterministic approach to uncertainty quantifications in non linear problems: application to fluid flow problems. Technical Report 00325315 Inria .
- Abgrall, R., Congedo, P.M., Geraci, G., 2014. A one-time truncate and encode multiresolution stochastic framework. *Journal of Computational Physics* 257, 19–56.
- Chen, Z., Huan, G., Ma, Y., 2006. Computational methods for multiphase flows in porous media. SIAM.
- Foo, J., Karniadakis, G.E., 2010. Multi-element probabilistic collocation method in high dimensions. *Journal of Computational Physics* 229, 1536–1557.
- Geraci, G., Congedo, P.M., Abgrall, R., Iaccarino, G., 2016. A novel weakly-intrusive non-linear multiresolution framework for uncertainty quantification in hyperbolic partial differential equations. *Journal of Scientific Computing* 66, 358–405.
- Jin, S., Pareschi, L., 2017. Uncertainty quantification for hyperbolic and kinetic equations. Springer.
- Lord, G.J., Powell, C.E., Shardlow, T., 2014. An introduction to computational stochastic PDEs. volume 50. Cambridge University Press.
- Maitre, O.P.L., Najm, H.N., Ghanem, R.G., Knio, O.M., 2004. Multi-resolution analysis of wiener-type uncertainty propagation schemes. *Journal of Computational Physics* 197, 502–531.
- Newsum, C.J., Powell, C.E., 2017. Efficient reduced basis methods for saddle point problems with applications in groundwater flow. *SIAM/ASA Journal on Uncertainty Quantification* 5, 1248–1278.
- Oliver, D.S., Reynolds, A.C., Liu, N., 2008. Inverse theory for petroleum reservoir characterization and history matching.
- Smith, R.C., 2013. Uncertainty quantification: theory, implementation, and applications. volume 12. Siam.

- Vauchel, N., Éric Garnier, Gomez, T., 2023. A multi-element non-intrusive polynomial chaos method using agglomerative clustering based on the derivatives to study irregular and discontinuous quantities of interest. *Journal of Computational Physics* 473.
- Wan, X., Karniadakis, G.E., 2006. Multi-element generalized polynomial chaos for bitrary probability measures. *SIAM Journal on Scientific Computing* 28, 901–928.
- Witteveen, J.A.S., Bijl, H., 2008. A monomial chaos approach for efficient uncertainty quantification in nonlinear problems. *SIAM Journal on Scientific Computing* 30, 1296–1317.
- Xiao, T., Kusch, J., Koellermeier, J., Frank, M., 2023. A flux reconstruction stochastic galerkin scheme for hyperbolic conservation laws. *Journal of Scientific Computing* 95.
- Xiu, D., 2010. Numerical methods for stochastic computations: a spectral method approach. Princeton university press.
- Yan, L., Shin, Y., Xiu, D., 2017. Sparse approximation using l1 - l2 minimization and its application to stochastic collocation. *SIAM Journal on Scientific Computing* 39, A229–A254.
- Yang, Z., Li, X., He, X., Ming, J., 2022. A stochastic collocation method based on sparse grids for a stochastic stokes-darcy model. *Discrete and Continuous Dynamical Systems - Series S* 15, 893–912.
- Zhang, Z., 2022. A physics-informed deep convolutional neural network for simulating and predicting transient darcy flows in heterogeneous reservoirs without labeled data. *Journal of Petroleum Science and Engineering* 211, 110179.
- Zhang, Z., Yan, X., Liu, P., Zhang, K., Han, R., Wang, S., 2023. A physics-informed convolutional neural network for the simulation and prediction of two-phase darcy flows in heterogeneous porous media. *Journal of Computational Physics* 477, 111919.
- Zhong, X., Shu, C.W., 2022. Entropy stable galerkin methods with suitable quadrature rules for hyperbolic systems with random inputs. *Journal of Scientific Computing* 92.